Computational and Structural Biotechnology Journal 21 (2023) 2631–2639

Contents lists available at ScienceDirect

Computational and Structural Biotechnology Journal

journal homepage: www.elsevier.com/locate/csbj

Research article

Metabolic reprogramming of cancer-associated fibroblasts in pancreatic cancer contributes to the intratumor heterogeneity of PET-CT

Qingcai Meng [a,b,c,d,1], Zengli Fang [a,b,c,d,1], Xiaoqi Mao [a,b,c,d,1], Rong Tang [a,b,c,d], Chen Liang [a,b,c,d], Jie Hua [a,b,c,d], Wei Wang [a,b,c,d], Si Shi [a,b,c,d], Xianjun Yu [a,b,c,d,*], Jin Xu [a,b,c,d,**]

[a] Department of Pancreatic Surgery, Fudan University Shanghai Cancer Center, Shanghai 200032, China
[b] Department of Oncology, Shanghai Medical College, Fudan University, Shanghai 200032, China
[c] Shanghai Pancreatic Cancer Institute, Shanghai 200032, China
[d] Pancreatic Cancer Institute, Fudan University, Shanghai 200032, China

ARTICLE INFO

Article history:
Received 2 December 2022
Received in revised form 21 March 2023
Accepted 6 April 2023
Available online 7 April 2023

Keywords:
Cancer-associated fibroblasts
Pancreatic cancer
PET-CT
Metabolic reprogramming

ABSTRACT

Intratumor heterogeneity of positron emission tomography-computed tomography (PET-CT) is reflected by variable ^{18}F-fluorodeoxyglucose (FDG) uptake. Increasing evidence has shown that neoplastic and non-neoplastic components can affect the total ^{18}F-FDG uptake in tumors. Cancer-associated fibroblasts (CAFs) is considered as the main non-neoplastic components in tumor microenvironment (TME) of pancreatic cancer. Our study aims to explore the impact of metabolic changes in CAFs on heterogeneity of PET-CT. A total of 126 patients with pancreatic cancer underwent PET-CT and endoscopic ultrasound elastography (EUS-EG) before treatment. High maximum standardized uptake value (SUVmax) from the PET-CT was positively correlated with the EUS-derived strain ratio (SR) and indicated poor prognosis of patients. In addition, single-cell RNA analysis showed that CAV1 affected glycolytic activity and correlated with glycolytic enzyme expression in fibroblasts in pancreatic cancer. We also observed the negative correlation between CAV1 and glycolytic enzyme expression in the tumor stroma by using immunohistochemistry (IHC) assay in the SUVmax-high and SUVmax-low groups of pancreatic cancer patients. Additionally, CAFs with high glycolytic activity contributed to pancreatic cancer cell migration, and blocking CAF glycolysis reversed this process, suggesting that glycolytic CAFs promote malignant biological behavior in pancreatic cancer. In summary, our research demonstrated that the metabolic reprogramming of CAFs affects total ^{18}F-FDG uptake in tumors. Thus, an increase in glycolytic CAFs with decreased CAV1 expression promotes tumor progression, and high SUVmax may be a marker for therapy targeting the neoplastic stroma. Further studies should clarify the underlying mechanisms.

© 2023 The Author(s). Published by Elsevier B.V. on behalf of Research Network of Computational and Structural Biotechnology. This is an open access article under the CC BY-NC-ND license (http://creativecommons.org/licenses/by-nc-nd/4.0/).

1. Introduction

As the most lethal gastrointestinal malignancy, pancreatic cancer is the fourth leading cause of cancer-related death worldwide, with a 5-year survival rate of approximately 9% [1]. The majority of patients with pancreatic cancer are diagnosed at an advanced stage, and only 20% of patients are eligible for curative surgery [2]. In addition, the current therapies for pancreatic cancer do not produce satisfactory results. Abundant stroma in the tumor microenvironment (TME) is a crucial feature of pancreatic cancer, and it contributes to tumor growth, progression and chemoresistance [3,4]. Therefore, further research on the TME of pancreatic cancer will help to explore new therapeutic strategies.

At present, two important clinical examinations, [^{18}F]-fluoro-2-deoxy-D-glucose (^{18}F-FDG) positron emission tomography-computed tomography (PET-CT) and endoscopic ultrasound (EUS), are used to diagnose pancreatic cancer. The standardized uptake value

* Correspondence to: Chief of the Chinese Study Group for Pancreatic Cancer (CSPAC); Chair of the Department of Pancreatic Surgery, Fudan University Shanghai Cancer Center; Director of the Pancreatic Cancer Institute, Fudan University, No. 270 Dong'An Road, Xuhui District, Shanghai 200032, China.
** Correspondence to: Department of Pancreatic Surgery, Fudan University Shanghai Cancer Center, No. 270 Dong'An Road, Xuhui District, Shanghai 200032, China.
E-mail addresses: yuxianjun@fudanpci.org (X. Yu), xujin@fudanpci.org (J. Xu).
[1] These authors contributed equally to this work and shared the first authorship.

https://doi.org/10.1016/j.csbj.2023.04.003
2001-0370/© 2023 The Author(s). Published by Elsevier B.V. on behalf of Research Network of Computational and Structural Biotechnology. This is an open access article under the CC BY-NC-ND license (http://creativecommons.org/licenses/by-nc-nd/4.0/).

(SUV) is a well-known measurement for ^{18}F-FDG uptake in PET-CT imaging. Increasing evidence shows that the SUVmax parameter, the largest SUV in the selected region, is an important prognostic factor [5–7]. EUS elastography (EUS-EG) has been used to detect the stiffness of the pancreas, and EUS-guided fine needle aspiration (EUS-FNA) has been employed to obtain tumor tissue [8]. The calculated strain ratio (SR) is a parameter derived from EUS-EG images and provides a quantitative measure of pancreatic tumor stiffness [9,10]. A previous study by our team showed that the SR value identified on EUS correlated with the stroma proportion and predicted the survival of pancreatic cancer patients treated with a nab-paclitaxel and gemcitabine regimen [11].

Metabolic reprogramming in tumors is a hot research topic, but few relevant studies have focused on the TME in pancreatic cancer. The cellular components of the TME include cancer-associated fibroblasts (CAFs), endothelial cells, immune inflammatory cells, and marrow-derived mesenchymal stem cells (MSCs) [12]. Recent studies have reported that FDG uptake might be increased in stromal cells in many tumors [13–16]. Hence, we aimed to explore the metabolic reprogramming of CAFs in pancreatic cancer.

2. Materials and methods

2.1. Study population

The 126 enrolled patients were histologically or cytologically diagnosed with either locally advanced pancreatic cancer (stage III, LAPC) or metastatic pancreatic cancer (stage IV, MPC) at the Fudan University Shanghai Cancer Center (FUSCC) from January 2018 to December 2020. All patients underwent EUS and ^{18}F-FDG PET-CT and only received gemcitabine (GEM)-based first-line chemotherapy. Clinical information on age, sex, tumor location, vascular involvement, lymph node or distant metastasis, and tumor markers (CA19–9, CA125, CA153, AFP, CEA) was extracted from our database. This study was approved by the Ethics Board of FUSCC, and due to its retrospective nature, the requirement for informed patient consent was waived.

2.2. EUS-EG

EUS-EG was conducted using a linear EUS scope (EG3870UTK; Pentax, Japan) combined with a HI VISION Preirus EUS system (Hitachi, Japan). The procedure was performed as previously described [11].

2.3. ^{18}F-FDG PET-CT

PET-CT was performed on a PET-CT scanner (Biograph Duo or Biograph TruePoint; Siemens Medical, Erlangen, Germany) at our institution. The SUVmax was calculated by identifying the area of most intense uptake using the Xeleris workstation. The PET-CT images were evaluated by two nuclear medicine physicians who were blinded to the clinical data.

2.4. Single-cell RNA analysis

The pancreatic cancer scRNA-seq datasets were downloaded from the Gene Expression Omnibus (GSE155698) and Genome Sequence Archive (AAD_CRA001160). The combination and analysis of the two scRNA-seq datasets were performed within the Seurat framework (4.2.0). Fibroblasts were selected based on their specific markers. The AUCell package was used to score the glycolytic activity of each fibroblast. The expression matrixes of two scRNA-seq datasets were integrated using the algorithm “Harmony” with the R package “harmony (0.1.1).

2.5. Immunohistochemistry (IHC)

Tumor tissues were obtained from pancreatic cancer patients who underwent PET-CT before treatment and underwent radical surgery at the FUSCC (n = 10). All procedures were performed after obtaining approval from the Clinical Research Ethics Committee of FUSCC, and informed consent was obtained from each patient prior to the analyses. The protocol was performed as previously described [17]. IHC staining with antibodies against CAV1 (#3238, CST), GLUT1 (66290–1-lg, Proteintech), HK2 (22029–1-AP, Proteintech), LDHA (19987–1-AP, Proteintech), and PKM2 (15822–1-AP, Proteintech) was performed to detect protein expression levels.

2.6. Cell lines and reagents

The human pancreatic cancer cell lines PANC-1 and SW1990 were obtained from American Type Culture Collection (ATCC). The culture conditions for all cells have been described previously [17,18]. Human CAFs were isolated from pancreatic cancer tissue from FUSCC. After excision, the tumor sample was immediately transported to the laboratory on ice. Next, the tissue sample was digested with 0.1% type I collagenase and trypsin. After filtering with a 400-mesh sieve, the cell suspension was centrifuged at 1,000g for 10 min. The isolated CAFs were tested for mycoplasma presence, verified by morphology and α-SMA expression analyses, and cultured in DMEM supplemented with 10% FBS. All cells were cultured in a humidified atmosphere in 5% CO2 at 37 °C. 2-Deoxy-D-glucose (2-DG), a glycolysis inhibitor (S4701), was obtained from Selleck (Houston, TX, USA).

2.7. Wound-healing assay

The cells were seeded into 6-well plates and grown to 90% confluence. The cell monolayer was scratched using a micropipette tip, and the cells were cultured in serum-free medium. Microphotographs were obtained at the indicated times.

2.8. Transwell migration assay

Cell migration assays were performed as previously described [17]. Cells were seeded in the upper chamber (approximately 6×10^4 cells) and cultured in 200 μl serum-free medium. The lower chamber was filled with 800 μl of medium containing 10% FBS. After the plate was cultured for 24 h, the lower surface of the plate containing cells was washed, and the cells were fixed, stained and imaged. The migrating cell number was determined in randomly selected fields.

2.9. Statistical methods

The data are presented as the mean ± SD. The relationships between clinicopathological characteristics were assessed using Spearman tests. The OS rates were assessed using Kaplan–Meier curves, and the differences between groups were compared using the log-rank test. Univariate and multivariate Cox proportional hazards models were applied using SPSS for Windows version 24.0 software (SPSS, Inc., Chicago, IL, USA). Differences with P values (two-sided) < 0.05 were considered statistically significant.

3. Results

3.1. Characteristics of patients

A total of 77 males and 49 females were enrolled in our study, with a median age of 60.8 years. The patients consisted of 59 LAPC and 67 MPC patients. The median tumor size, SUVmax and EUS-SR of the primary lesions were 35.9, 7.1 and 41.9, respectively, with ranges

Table 1
Demographic details of patients included in study.

Characteristic	Total (N = 126)
Median age (years)	60.8 (30–83)
Sex (%)	
male	77 (61%)
female	49 (39%)
Tumour location (%)	
Head	79 (63%)
Body and tail	47 (37%)
Median tumor size (mm)	35.9 (11–99.3)
Lymph nodes metastasis (%)	
Yes	108 (86%)
No	18 (14%)
Distant metastasis (%)	
Yes	59 (47%)
No	66 (53%)
Vascular involvement (%)	
Yes	111 (88%)
No	15 (22%)
Median SUVmax (range)	7.1 (0–27.1)
Median EUS-SR (range)	41.9 (7.9–124.7)
Median tumor marker level pre-treatment (range)	
CA19–9	917.8 (1.5–10000)
CA125	105.3 (5.8–5000)
CA153	19.3 (2.3–273)
AFP	5.5 (0.95–157.3)
CEA	23.8 (0.34–855)

Table 2
Median SUVmax related to other characteristics.

Characteristic	Median SUVmax	p-value
Median age (years)		0.309
≥ 60	6.7	
< 60	7.5	
Sex		0.962
male	7.1	
female	7.0	
Tumour location		0.706
Head	6.9	
Body and tail	7.2	
Median tumor size (mm)		0.003
≥ 40	8.6	
< 40	6.2	
Lymph nodes metastasis		0.002
Yes	7.5	
No	4.2	
Distant metastasis		0.002
Yes	8.3	
No	5.9	
Vascular involvement		0.012
Yes	7.4	
No	4.3	
Median EUS-SR		0.004
≥ 40	8.1	
< 40	5.9	

of 11–99.3, 0–27.1 and 7.9–124.7. Overall, 111 patients (88%) were found to have lymph node metastasis, and 108 patients (86%) were found to have vascular involvement. All patients underwent PET-CT and EUS and received a GEM-based first-line regimen. The clinical characteristics of the patients are described in Table 1. The median overall survival (OS) was 8.9 (range 4–24) months.

3.2. Correlation of SUVmax with duration of survival

The SUV is a well-known measurement for ^{18}F-FDG uptake and the SUVmax is the largest value in the selected region of interest the trans-axial PET image. Next, we explored the correlation between SUVmax and other characteristics of patients with pancreatic cancer using Spearman tests. A high SUVmax was associated with tumor size, vascular involvement, EUS-SR, and lymph node and distant metastasis but not with sex, age or tumor location (Table 2). There was a positive correlation between SUVmax and SR (Fig. 1**A**). A scatter plot of the relationship of SUVmax with SR is shown in Fig. 1**B** (R= 0.298, $P < 0.001$). All factors associated with survival in the univariate analysis are shown in Table 3. There was a significant association of tumor size (> 3 cm), SUVmax (> 6.4), SR (> 40.33), CA19–9 (> 246 U/ml), CA125 (> 27.9 U/ml), CA153 (> 12 U/ml), vascular involvement, lymph node metastasis and distant metastasis with poor OS. In addition, cumulative survival was significantly better in patients in the low SUVmax group (9.8 months for SUVmax < 6 versus 8.2 months for SUVmax ≥ 6, $p < 0.01$; Fig. 1**C**). The relationship of cumulative survival with EUS-SR is shown in Fig. 1**D** (10.1 months for SR < 40 versus 7.8 months for SR ≥ 40, $p < 0.01$). The characteristics significantly correlated with OS in the univariate analysis were entered into the multivariate analysis. The multivariate Cox regression analysis showed that tumor size, vascular involvement, distant metastasis, CA19–9 and SR were significant prognostic factors for OS.

3.3. Metabolic reprogramming of CAFs in pancreatic cancer affects the heterogeneity of PET-CT

Both neoplastic and non-neoplastic components can affect the total ^{18}F-FDG uptake of PET-CT in malignant tumors. Similar research has showed that ^{18}F-FDG preferentially accumulates in α-SMA-positive myofibroblasts in tumor model [19]. Recent study also showed that CAFs may influence ^{18}F-FDG uptake in PET-CT imaging [20]. Our previous study showed that the glucose metabolism in pancreatic cancer cells was associated with the SUVmax in PET-CT scan[21]. In this study, we explored the role of CAFs on ^{18}F-FDG uptake of PET-CT imaging in pancreatic cancer. The pancreatic cancer scRNA-seq datasets were downloaded from the Gene Expression Omnibus (GSE155698) and Genome Sequence Archive (AAD_CRA001160). The combination and analysis of the two scRNA-seq datasets were performed within the Seurat framework (4.2.0). Fibroblasts were selected based on their specific markers. We first annotated all cells according to their specific markers as shown in supplementary Fig. 1 A. Then, we isolated fibroblast as a new Seurat object and visualize it as shown in supplementary Fig. 1B according to the fibroblast marker (DCN, TAGLN, COL3A1, COL1A1, FAP and CAV1). A dot plot showing the distribution of common fibroblast markers in selected pancreatic cancer-infiltrating fibroblasts was generated (Fig. 2). A UMAP plot showing six subclusters for the selected fibroblasts was created (Fig. 3A). Furthermore, the AUCell package was used to score the glycolytic activity of each fibroblast, and the fibroblast cells of subcluster 3 showed higher glycolytic activity (Fig. 3B). Caveolin-1 (CAV1), as one of the main indicators of CAF activation, was expressed at low levels in cells of subcluster 3 with a high glycolysis score (Fig. 3C). Next, we analyzed the correlation between the expression of CAV1 and glycolytic enzymes in CAFs. As shown in Fig. 4A, glycolytic enzymes, including PKM2, HK2, PGK1 and HOMER1, were highly expressed in CAFs with low CAV1 expression, suggesting that CAV1 is involved in the metabolic alteration of CAFs to favor the Warburg effect. To further verify the conclusions, we detected the expression of the above proteins in the SUVmax-high and SUVmax-low groups of pancreatic cancer patients and observed a negative correlation between CAV1 and glycolytic enzyme expression in the tumor stroma (Fig. 4B). The above results further confirmed that glucose metabolic reprogramming of CAFs in pancreatic cancer affects the heterogeneity of PET-CT.

3.4. Blocking CAF glycolysis affects the progression of pancreatic cancer

To investigate the role of CAF glycolysis in pancreatic cancer progression, we next pretreated CAFs with 2-DG, a glycolysis inhibitor, and cocultured them with pancreatic cancer cells. Wound-

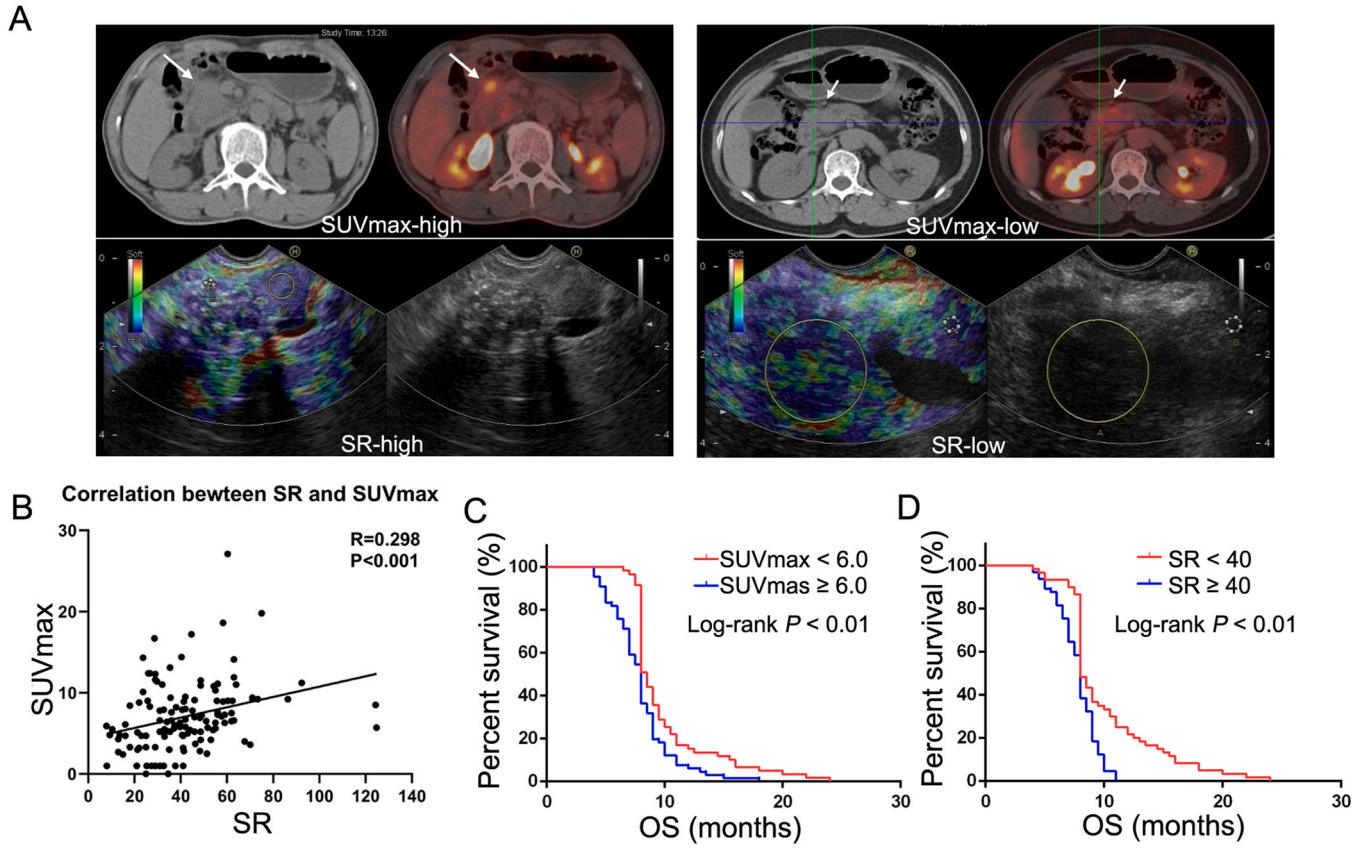

Fig. 1. The correlation between SUVmax and EUS-SR. **A.** Sample graph of PET-CT and EUS-SR. **B.** There was a positive correlation between SUVmax and SR. A scatter plot of the relationship between SUVmax and SR is shown (Spearman's R= 0.298, $p < 0.01$).

healing assays revealed that the increase in cancer cell migration induced by CAFs was reversed in by 2-DG (Fig. 5**A-B**). Moreover, in vitro transwell assays indicated that the number of migrating cells was significantly increased in the CAF group, and CAF glycolysis inhibition decreased the progression of pancreatic cancer (Fig. 5**C-D**).

4. Discussion

^{18}F-FDG PET-CT has been routinely used for cancer diagnosis, staging and therapeutic response monitoring. Clinical studies have demonstrated that ^{18}F-FDG uptake reflects metabolic activity and is closely correlated with glucose metabolism in many malignant tumors. SUVmax has been shown to be a surrogate marker for prognosis. However, the major factors affecting ^{18}F-FDG accumulation in pancreatic cancer have not been fully elucidated. The thick desmoplastic stroma is one of the defining features of pancreatic cancer, and the highly heterogeneous stroma consists of CAFs, immune cells, blood vessels and extracellular matrix[22]. Many studies have proposed that CAFs are involved in energy metabolism in tumor cells [23,24]. Hence, this study aimed to explore the potential effect of CAF glycolysis on tumors.

Intratumor heterogeneity of PET-CT is reflected by variation in ^{18}F-FDG uptake. Consistent with our conclusion, the SUV derived from PET-CT has been suggested to be related to the distribution of different tissue components in the tumor and clinical parameters, including tumor size, angiogenesis, histological grade and tumor growth pattern[25–27]. The SR obtained by EUS-EG provides a quantitative measure of tumor stiffness related to stromal proportion in pancreatic cancer. Our previous study demonstrated that the SR was correlated with the stroma proportion and predicted the survival of pancreatic cancer patients[11]. In this study, we also clearly demonstrated that both high PET-CT-derived SUVmax and SR predicted poor OS. Interestingly, this is the first study to propose a significant and positive correlation between SUVmax and SR. We wondered whether the rich stroma of the pancreas affects the metabolic changes in tumors. Many controversial roles of the stroma in tumors have been proposed. The stroma in tumors was found to be closely correlated with ^{18}F-FDG uptake, likely because it influences angiogenesis, microvessel density, and nutrient and oxygen supply [28–30]. Similarly, the nonneoplastic components in tumors have been shown to contribute to total ^{18}F-FDG uptake. ^{18}F-FDG accumulates predominantly in the nonneoplastic stroma, especially in α-SMA-positive myofibroblasts, in various malignant tumor models [19,31,32]. As CAFs are the major component of the tumor stroma, these findings suggest that glycolytic CAFs increase the total ^{18}F-FDG uptake in tumors, and high PET-CT-derived SUVmax may be a marker for therapy targeting the neoplastic stroma. Moreover, there are several possible mechanisms accounting for the impact of CAFs with high glycolysis on killing function of cytotoxic T lymphocytes (CTLs) in dense ECM. On the one hand, an increased rate of glycolytic metabolism within the TME induced by CAFs can lead to glucose deficiency, which contributes to a competitive struggling between cancer cells with CTLs. In such conditions, CTLs tend to decrease their number[33]. On the other hand, some CAF-derived secretory proteins, such as βig-h3, can decrease the transduction of T cell receptor (TCR) signaling via binding to the surface marker of CTLs[34]. Moreover, CAFs can also contribute to CTL killing in an antigen-dependent mechanism by activating PD-L2 an FasL[35].

Previous studies have reported that CAV1 increases tumor cell glucose uptake, lactate output and proliferation[36,37]. Recently, CAV1 was shown to be involved in metabolic reprogramming in fibroblasts[38–40]. In our study, single-cell RNA analysis and IHC assays showed that CAV1 affected glycolytic activity, and CAV1

Table 3
Univariate and multivariate analysis of characteristics for survival.

Characteristics	Univariate			Multivariate		
	HR	95% CI	P value	HR	95% CI	P value
Age (years)						
≤ 60	1.07	0.75–1.53	0.71			
> 60						
Gender						
Male	0.81	0.57–1.17	0.27			
Female						
Tumor location						
Head	0.83	0.58–1.21	0.33			
Body and Tail						
Tumor size (cm)						
≤ 3	0.66	0.45–0.96	0.03	0.63	0.42–0.95	0.03
> 3						
SR						
≤ 40.33	0.51	0.34–0.75	< 0.01	0.62	0.41–0.92	0.02
> 40.33						
SUVmax						
≤ 6.4	0.61	0.43–0.88	< 0.01	0.81	0.55–1.19	0.28
> 6.4						
CA19–9 (U/ml)						
≤ 246	0.51	0.35–0.74	< 0.01	1.93	1.28–2.92	< 0.01
> 246						
Metastasis						
No	0.41	0.28–0.60	< 0.01	0.48	0.32–0.71	< 0.01
Yes						
vascular involvement						
No	0.40	0.21–0.76	< 0.01	0.58	0.29–1.16	0.13
Yes						
LN metastasis						
No	0.50	0.29–0.86	0.01	0.78	0.43–1.42	0.424
Yes						
CA125						
≤ 27.9	0.53	0.36–0.77	< 0.01	0.72	0.48–1.07	0.1
> 27.9						
CA153						
≤ 12	0.68	0.48–0.98	0.04	0.83	0.57–1.21	0.34
> 12						
AFP						
≤ 2.73	0.89	0.62–1.26	0.50			
> 2.73						
CEA						
≤ 5.2	0.72	0.50–1.02	0.07			
> 5.2						

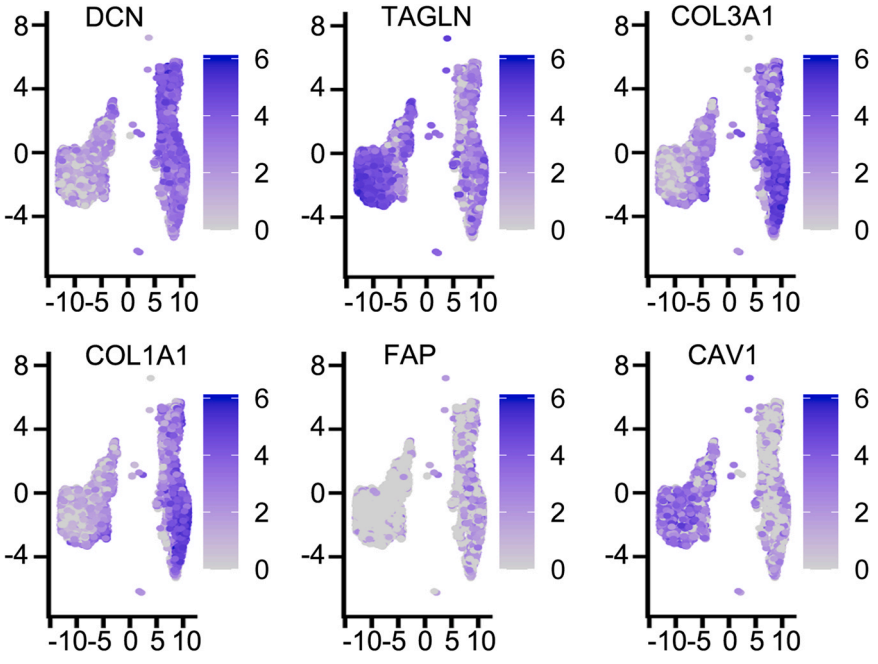

Fig. 2. Dot plot showing the distribution of common fibroblast markers (DCN, TAGLN, COL3A1, COL1A1, FAP and CAV1) in selected pancreatic cancer-infiltrating fibroblasts.

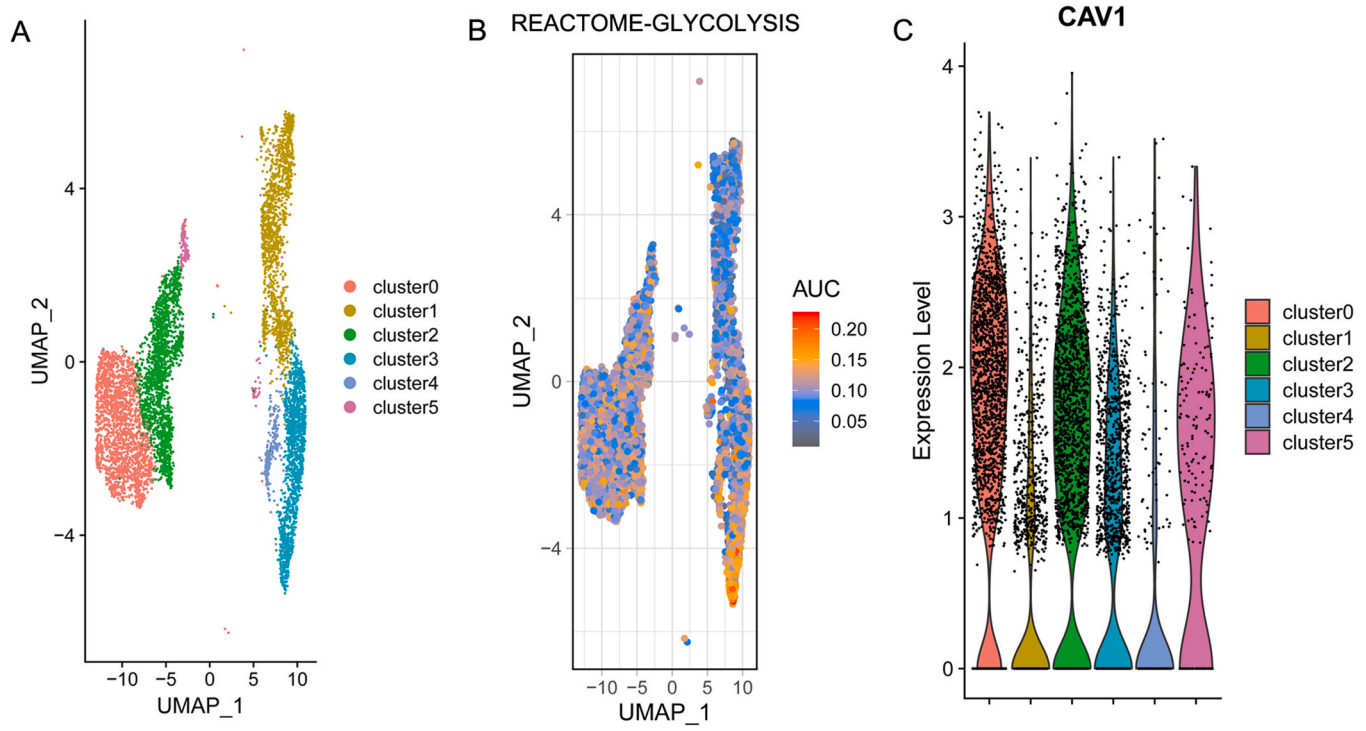

Fig. 3. Single-cell RNA analysis of CAFs in pancreatic cancer. **A**. UMAP plot showing the subclusters of selected fibroblasts. **B**. UMAP plot showing the relative glycolytic activity of each cell. **C**. Expression of CAV1 in each subcluster of fibroblasts.

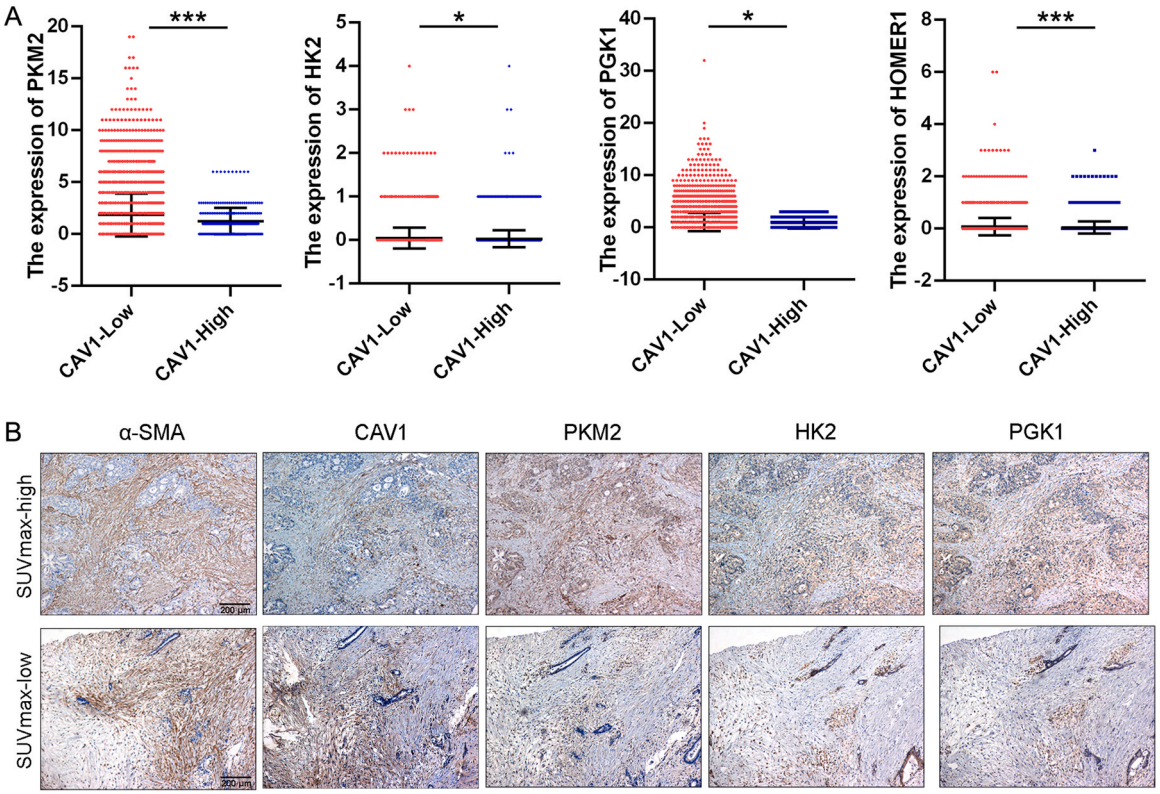

Fig. 4. The expression of CAV1 was related to CAF glycolysis. **A.** Negative association between glycolytic enzyme and CAV1 expression in CAFs (* $p < 0.05$, *** $p < 0.001$). **B.** Negative correlation between CAV1 and glycolytic enzyme expression in the tumor stroma as determined by IHC.

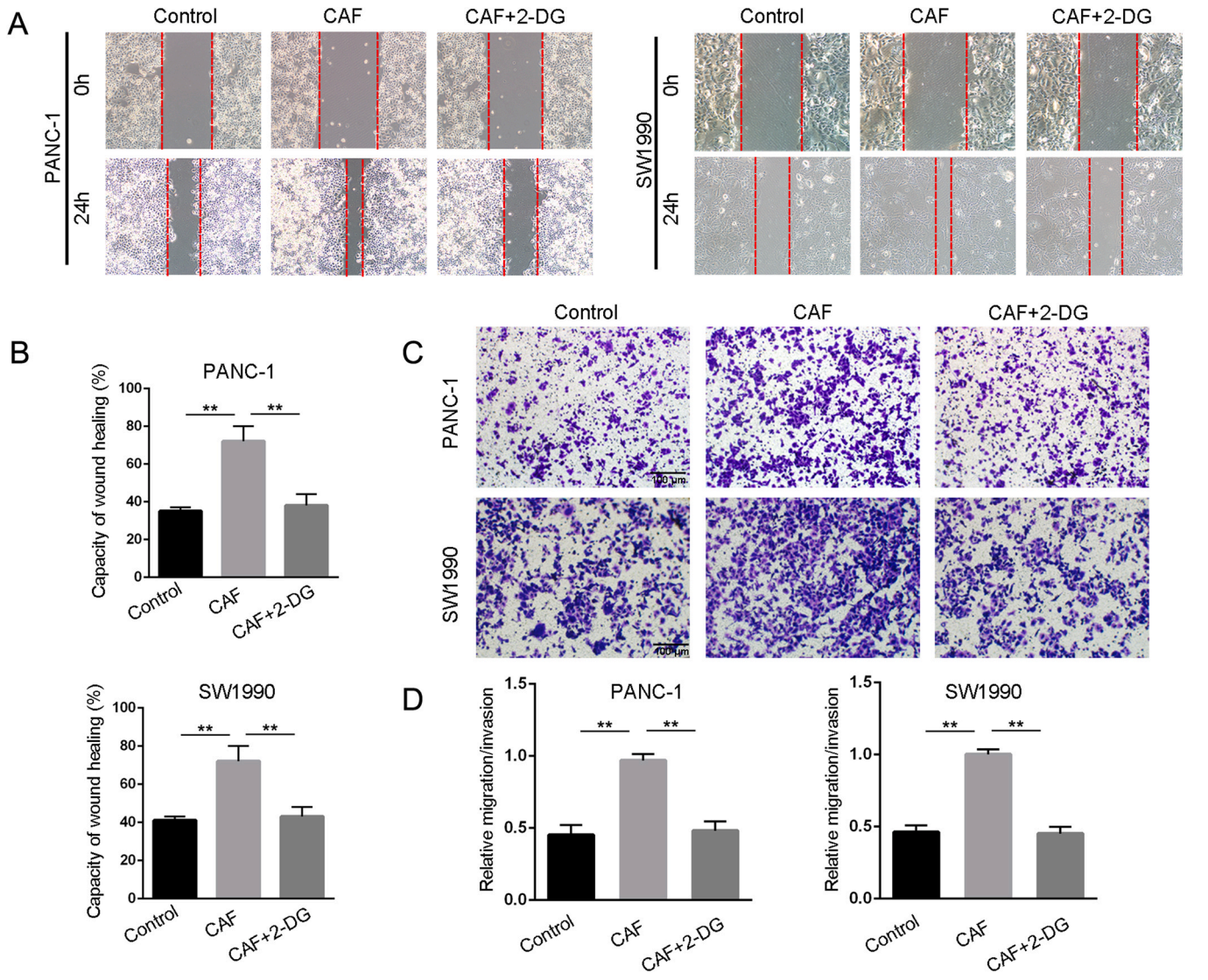

Fig. 5. Blocking CAF glycolysis affected pancreatic cancer progression. **A-B**. Analysis of the effect of CAF glycolysis on wound closure as determined by wound-healing assay (200 ×, ** $p < 0.01$). **C-D.** Analysis of the effect of CAF glycolysis on migration capacity as determined by in vitro transwell migration assays (scale bar 100 μm, ** $p < 0.01$). CAFs were cocultured with pancreatic cancer cells after treatment with the glycolytic inhibitor 2-DG for 24 h.

expression was correlated with glycolytic enzyme expression in fibroblasts in pancreatic cancer. Similarly, several glycolytic enzymes, including PGK1, PKM2, aldolase A, enolase 1, and LDHA, were upregulated in bone marrow-derived stromal cells from Cav1-knockout mice[41]. In addition, it has been shown that CAV1-deficient stromal fibroblasts surrounding malignant cells promote aerobic glycolysis with a simultaneous increase in mitochondrial activity and enhance angiogenesis by recruiting CAV1-positive microvascular cells [38,40,42].

The metabolic crosstalk between CAFs and tumor cells depends on the amount of oxygen, availability of extracellular metabolites and regulation of signaling molecules. Metabolic reprogramming of CAFs promotes the growth of tumor cells, which is considered reversed metabolic symbiosis[43]. Moreover, CAV1 expression in CAFs was found to promote CAF contractility and the migration and invasiveness of carcinoma cells[44]. Similarly, in the present study, CAFs with high glycolytic activity contributed to pancreatic cancer cell migration, and blocking CAF glycolysis reversed this process. However, the potential regulatory mechanism is still unclear. Interestingly, CAV1 is believed to regulate constitutive activation of CAFs in fibrotic diseases by preventing collagen deposition, fibroblast proliferation and TGF-β signaling via the PI3K/AKT, MAPK, Rho-like GTPase, or JNK pathways[39,45]. Furthermore, CAF subpopulations existing in the tumor stroma play different roles according to their CAV1 expression[46].

The present study had several potential limitations. First, the number of samples used in this study was small, and further large-scale prospective studies are needed. Second, patients with pancreatic cancer were not included in the surgical resection group, and thus, the results may be biased. Third, the mechanism by which CAV1 affects CAF glycolysis remains unclear, and additional clinical and basic research studies are needed.

5. Conclusion

In conclusion, our research demonstrated that SUVmax was positively associated with EUS-SR in pancreatic cancer. Increased numbers of glycolytic CAFs with decreased CAV1 expression promoted tumor progression, and high SUVmax may be a marker for therapy targeting the neoplastic stroma. Further studies should be helpful to clarify the underlying mechanisms.

Ethical approval

The Institutional Research Ethics Committee of FUSCC approved this study, and written informed consent was obtained from all patients prior to the investigation. We confirmed that the experiments on human tissue samples were performed in accordance with relevant guidelines and regulations.

Funding

This study was jointly supported by the National Natural Science Foundation of China (No. 82002541), the Shanghai Sailing Program (No. 20YF1409000), Scientific Innovation Project of Shanghai Education Committee (2019–01–07–00–07-E00057), Clinical Research Plan of Shanghai Hospital Development Center (SHDC2020CR1006A), and Xuhui District Artificial Intelligence Medical Hospital Cooperation Project (2021–011).

CRediT authorship contribution statement

QCM and RT performed the bioinformatic analysis. ZLF and XQM cultured the cancer cells and performed the functional experiments. CL and JH carried out the IHC assays. QCM and WW performed the statistical analyses. QCM, SS and JX designed the study. JX and XJY revised the manuscript. All authors read and approved the final manuscript.

Declaration of Competing Interest

The authors declare that they have no known competing financial interests or personal relationships that could have appeared to influence the work reported in this paper.

Acknowledgment

Not applicable.

Appendix A. Supporting information

Supplementary data associated with this article can be found in the online version at doi:10.1016/j.csbj.2023.04.003.

References

[1] Siegel RL, Miller KD, Fuchs HE, Jemal A. Cancer Statistics, 2021. CA Cancer J Clin 2021;71(1):7–33.
[2] Hidalgo M. Pancreatic cancer. N Engl J Med 2010;362(17):1605–17.
[3] Erkan M, Michalski CW, Rieder S, Reiser-Erkan C, Abiatari I, Kolb A, et al. The activated stroma index is a novel and independent prognostic marker in pancreatic ductal adenocarcinoma. Clin Gastroenterol Hepatol 2008;6(10):1155–61.
[4] Neesse A, Algul H, Tuveson DA, Gress TM. Stromal biology and therapy in pancreatic cancer: a changing paradigm. Gut 2015;64(9):1476–84.
[5] Kurtipek E, Cayci M, Duzgun N, Esme H, Terzi Y, Bakdik S, et al. (18)F-FDG PET/CT mean SUV and metabolic tumor volume for mean survival time in non-small cell lung cancer. Clin Nucl Med 2015;40(6):459–63.
[6] Xu HX, Chen T, Wang WQ, Wu CT, Liu C, Long J, et al. Metabolic tumour burden assessed by (1)(8)F-FDG PET/CT associated with serum CA19-9 predicts pancreatic cancer outcome after resection. Eur J Nucl Med Mol Imaging 2014;41(6):1093–102.
[7] Zhu D, Wang L, Zhang H, Chen J, Wang Y, Byanju S, et al. Prognostic value of 18F-FDG-PET/CT parameters in patients with pancreatic carcinoma: a systematic review and meta-analysis. Med (Baltim) 2017;96(33):e7813.
[8] Banafea O, Mghanga FP, Zhao J, Zhao R, Zhu L. Endoscopic ultrasonography with fine-needle aspiration for histological diagnosis of solid pancreatic masses: a meta-analysis of diagnostic accuracy studies. BMC Gastroenterol 2016;16:108.
[9] Dawwas MF, Taha H, Leeds JS, Nayar MK, Oppong KW. Diagnostic accuracy of quantitative EUS elastography for discriminating malignant from benign solid pancreatic masses: a prospective, single-center study. Gastrointest Endosc 2012;76(5):953–61.
[10] Itokawa F, Itoi T, Sofuni A, Kurihara T, Tsuchiya T, Ishii K, et al. EUS elastography combined with the strain ratio of tissue elasticity for diagnosis of solid pancreatic masses. J Gastroenterol 2011;46(6):843–53.
[11] Shi S, Liang C, Xu J, Meng Q, Hua J, Yang X, et al. The strain ratio as obtained by endoscopic ultrasonography elastography correlates with the stroma proportion and the prognosis of local pancreatic cancer. Ann Surg 2020;271(3):559–65.
[12] Sun Q, Zhang B, Hu Q, Qin Y, Xu W, Liu W, et al. The impact of cancer-associated fibroblasts on major hallmarks of pancreatic cancer. Theranostics 2018;8(18):5072–87.
[13] Chiarugi P, Cirri P. Metabolic exchanges within tumor microenvironment. Cancer Lett 2016;380(1):272–80.
[14] Migneco G, Whitaker-Menezes D, Chiavarina B, Castello-Cros R, Pavlides S, Pestell RG, et al. Glycolytic cancer associated fibroblasts promote breast cancer tumor growth, without a measurable increase in angiogenesis: evidence for stromal-epithelial metabolic coupling. Cell Cycle 2010;9(12):2412–22.
[15] Sanita P, Capulli M, Teti A, Galatioto GP, Vicentini C, Chiarugi P, et al. Tumor-stroma metabolic relationship based on lactate shuttle can sustain prostate cancer progression. BMC Cancer 2014;14:154.
[16] Zhang D, Wang Y, Shi Z, Liu J, Sun P, Hou X, et al. Metabolic reprogramming of cancer-associated fibroblasts by IDH3alpha downregulation. Cell Rep 2015;10(8):1335–48.
[17] Meng Q, Shi S, Liang C, Liang D, Hua J, Zhang B, et al. Abrogation of glutathione peroxidase-1 drives EMT and chemoresistance in pancreatic cancer by activating ROS-mediated Akt/GSK3beta/Snail signaling. Oncogene 2018;37(44):5843–57.
[18] Meng Q, Liang C, Hua J, Zhang B, Liu J, Zhang Y, et al. A miR-146a-5p/TRAF6/NF-kB p65 axis regulates pancreatic cancer chemoresistance: functional validation and clinical significance. Theranostics 2020;10(9):3967–79.
[19] Sun YL, Jan ML, Kao PF, Fan KH, Hsu HT, Chang WC, et al. Coincidence planar imaging for dynamic [18F]FDG uptake in nude mice with tumors and inflammation: correlated with histopathology and micro-autoradiography. Kaohsiung J Med Sci 2005;21(6):258–66.
[20] Shangguan C, Gan G, Zhang J, Wu J, Miao Y, Zhang M, et al. Cancer-associated fibroblasts enhance tumor (18)F-FDG uptake and contribute to the intratumor heterogeneity of PET-CT. Theranostics 2018;8(5):1376–88.
[21] Ji S, Qin Y, Liang C, Huang R, Shi S, Liu J, et al. FBW7 (F-box and WD Repeat Domain-Containing 7) negatively regulates glucose metabolism by targeting the c-Myc/TXNIP (Thioredoxin-Binding Protein) axis in pancreatic cancer. Clin Cancer Res 2016;22(15):3950–60.
[22] Chu GC, Kimmelman AC, Hezel AF, DePinho RA. Stromal biology of pancreatic cancer. J Cell Biochem 2007;101(4):887–907.
[23] Balliet RM, Capparelli C, Guido C, Pestell TG, Martinez-Outschoorn UE, Lin Z, et al. Mitochondrial oxidative stress in cancer-associated fibroblasts drives lactate production, promoting breast cancer tumor growth: understanding the aging and cancer connection. Cell Cycle 2011;10(23):4065–73.
[24] Pavlides S, Tsirigos A, Vera I, Flomenberg N, Frank PG, Casimiro MC, et al. Loss of stromal caveolin-1 leads to oxidative stress, mimics hypoxia and drives inflammation in the tumor microenvironment, conferring the "reverse Warburg effect": a transcriptional informatics analysis with validation. Cell Cycle 2010;9(11):2201–19.
[25] Fujii T, Yajima R, Kurozumi S, Higuchi T, Obayashi S, Tokiniwa H, et al. Clinical significance of 18F-FDG-PET in invasive lobular carcinoma. Anticancer Res 2016;36(10):5481–5.
[26] Kitagawa Y, Sano K, Nishizawa S, Nakamura M, Ogasawara T, Sadato N, et al. FDG-PET for prediction of tumour aggressiveness and response to intra-arterial chemotherapy and radiotherapy in head and neck cancer. Eur J Nucl Med Mol Imaging 2003;30(1):63–71.
[27] Lee DS, Kim SJ, Jang HS, Yoo IR, Park KR, Na SJ, et al. Clinical correlation between tumor maximal standardized uptake value in metabolic imaging and metastatic tumor characteristics in advanced non-small cell lung cancer. Med (Baltim) 2015;94(32):e1304.
[28] Kaira K, Endo M, Abe M, Nakagawa K, Ohde Y, Okumura T, et al. Biologic correlation of 2-[18F]-fluoro-2-deoxy-D-glucose uptake on positron emission tomography in thymic epithelial tumors. J Clin Oncol 2010;28(23):3746–53.
[29] Kawada K, Nakamoto Y, Kawada M, Hida K, Matsumoto T, Murakami T, et al. Relationship between 18F-fluorodeoxyglucose accumulation and KRAS/BRAF mutations in colorectal cancer. Clin Cancer Res 2012;18(6):1696–703.
[30] Mizuno T, Kamai T, Abe H, Sakamoto S, Kitajima K, Nishihara D, et al. Clinically significant association between the maximum standardized uptake value on 18F-FDG PET and expression of phosphorylated Akt and S6 kinase for prediction of the biological characteristics of renal cell cancer. BMC Cancer 2015;15:1097.
[31] Wang Y, Gan G, Wang B, Wu J, Cao Y, Zhu D, et al. Cancer-associated fibroblasts promote irradiated cancer cell recovery through autophagy. EBioMedicine 2017;17:45–56.
[32] Yamato M, Kataoka Y, Mizuma H, Wada Y, Watanabe Y. PET and macro- and microautoradiographic studies combined with immunohistochemistry for monitoring rat intestinal ulceration and healing processes. J Nucl Med 2009;50(2):266–73.
[33] Kato T, Noma K, Ohara T, Kashima H, Katsura Y, Sato H, et al. Cancer-associated fibroblasts affect intratumoral CD8(+) and FoxP3(+) T cells via IL6 in the tumor microenvironment. Clin Cancer Res 2018;24(19):4820–33.
[34] Goehrig D, Nigri J, Samain R, Wu Z, Cappello P, Gabiane G, et al. Stromal protein betaig-h3 reprogrammes tumour microenvironment in pancreatic cancer. Gut 2019;68(4):693–707.
[35] Lakins MA, Ghorani E, Munir H, Martins CP, Shields JD. Cancer-associated fibroblasts induce antigen-specific deletion of CD8 (+) T Cells to protect tumour cells. Nat Commun 2018;9(1):948.
[36] Salani B, Maffioli S, Hamoudane M, Parodi A, Ravera S, Passalacqua M, et al. Caveolin-1 is essential for metformin inhibitory effect on IGF1 action in non-small-cell lung cancer cells. FASEB J 2012;26(2):788–98.

[37] Tahir SA, Yang G, Goltsov A, Song KD, Ren C, Wang J, et al. Caveolin-1-LRP6 signaling module stimulates aerobic glycolysis in prostate cancer. Cancer Res 2013;73(6):1900–11.
[38] Bonuccelli G, Whitaker-Menezes D, Castello-Cros R, Pavlides S, Pestell RG, Fatatis A, et al. The reverse Warburg effect: glycolysis inhibitors prevent the tumor promoting effects of caveolin-1 deficient cancer associated fibroblasts. Cell Cycle 2010;9(10):1960–71.
[39] Shihata WA, Putra MRA, Chin-Dusting JPF. Is there a potential therapeutic role for caveolin-1 in fibrosis? Front Pharm 2017;8:567.
[40] Wu KN, Queenan M, Brody JR, Potoczek M, Sotgia F, Lisanti MP, et al. Loss of stromal caveolin-1 expression in malignant melanoma metastases predicts poor survival. Cell Cycle 2011;10(24):4250–5.
[41] Pavlides S, Whitaker-Menezes D, Castello-Cros R, Flomenberg N, Witkiewicz AK, Frank PG, et al. The reverse Warburg effect: aerobic glycolysis in cancer associated fibroblasts and the tumor stroma. Cell Cycle 2009;8(23):3984–4001.
[42] Dimmer KS, Friedrich B, Lang F, Deitmer JW, Broer S. The low-affinity monocarboxylate transporter MCT4 is adapted to the export of lactate in highly glycolytic cells. *Biochem J* 2000;350(Pt 1):219–27.
[43] Kumar D, New J, Vishwakarma V, Joshi R, Enders J, Lin F, et al. Cancer-Associated Fibroblasts Drive Glycolysis in a Targetable Signaling Loop Implicated in Head and Neck Squamous Cell Carcinoma Progression. Cancer Res 2018;78(14):3769–82.
[44] Goetz JG, Minguet S, Navarro-Lerida I, Lazcano JJ, Samaniego R, Calvo E, et al. Biomechanical remodeling of the microenvironment by stromal caveolin-1 favors tumor invasion and metastasis. Cell 2011;146(1):148–63.
[45] Arcucci A, Ruocco MR, Amatruda N, Riccio A, Tarantino G, Albano F, et al. Analysis of extracellular superoxide dismutase in fibroblasts from patients with systemic sclerosis. J Biol Regul Homeost Agents 2011;25(4):647–54.
[46] Raudenska M, Gumulec J, Balvan J, Masarik M. Caveolin-1 in oncogenic metabolic symbiosis. Int J Cancer 2020;147(7):1793–807.